Photodissociation of Nitric Oxide from Nitrosyl Metalloporphyrins in Micellar Solutions

Haruna Adachi, Hirotaka Sonoki, Mikio Hoshino,* Masanobu Wakasa, and Hisaharu Hayashi

The Institute of Physical and Chemical Research, Wako, Saitama 351-0198, Japan

Yoshio Miyazaki

Department of Chemistry, Faculty of Engineering, Toyo University, Kujirai, Kawagoe, Saitama 350-8585, Japan

Received: July 13, 2000; In Final Form: October 18, 2000

Laser-photolysis studies of nitrosyl metalloporphyrins (MP), (NO)Fe^{II}Hem (Hem = protoporphyrin IX), (NO)-Co^{II}OEP (OEP = octaethylporphyrin), and (NO)Mn^{II}TPP (TPP = tetraphenylporphyrin), in aqueous ionic micellar solutions were carried out. The nitrosyl porphyrins in the micellar solutions readily photodissociate NO, leaving the MP in micelles: the quantum yields are 0.15 (±0.1) for (NO)Fe^{II}Hem, 0.55 (±0.05) for (NO)Co^{II}OEP, and 0.21 (±0.02) for (NO)Mn^{II}TPP. The MP thus produced recombine with NO to regenerate the parent nitrosyl porphyrins. The decay of MP in the absence of the excess NO follows second-order kinetics with the rate constant k_{MNO}(second) (MNO = FeNO, CoNO, and MnNO). In the presence of excess NO, the decay of MP follows pseudo-first-order kinetics with the rate constant k_M (M = Fe, Co, and Mn). The value of k_M was measured as a function of [NO]. For Fe^{II}Hem and Co^{II}OEP, the plots of k_{Co} vs [NO] and k_{Fe} vs [NO] gave straight lines. The slopes of the lines obtained with Fe^{II}Hem and Co^{II}OEP afford the bimolecular rate constants k_{FeNO}(pseudo) and k_{CoNO}(pseudo), respectively. It is found that k_{FeNO}(pseudo) > k_{FeNO}(second) and k_{CoNO}(pseudo) > k_{CoNO}(second). The differences between k_{MNO}(pseudo) and k_{MNO}(second) observed for Fe^{II}Hem and Co^{II}OEP are interpreted by assuming that (1) NO molecules in the micellar solutions are dissolved in both micelles and the aqueous phase and (2) NO molecules trapped in micelles hardly react with MP because of the electrostatic repulsion between ionic micelles. In the case of Mn^{II}TPP, the pseudo-first-order rate constant, k_{Mn}, is found to asymptotically increase with an increase in [NO] to a limiting value. The reaction mechanisms for the nitrosylation of MP in micellar solutions are discussed in detail on the basis of the kinetic studies.

Introduction

Metalloporphyrins (MP) with simple diatomic molecules at the axial positions have been extensively studied for the elucidation of the functions and reactions of hemeproteins in vivo.[1−12] Particular attention has been paid to the dioxygen and carbon monoxide adducts of MP.[1−4,6−9] Recent advances in medical science reveal that NO plays a key role in vivo as a bioregulatory molecule in blood pressure control,[13,14] neuronal transmission,[15,16] and immune response.[17,18] Because NO readily reacts with metalloenzymes and hemeproteins to give their NO adducts,[19−21] the studies of nitrosyl complexes in chemistry are increasingly important in relation to the understanding of the biological functions of NO.

NO adducts of synthetic MP with central metals Fe^{II}, Co^{II}, and Mn^{II} in organic solutions efficiently undergo photochemical dissociation of NO to yield the MP,[2,5] which readily return to the nitrosyl adducts by the recombination reaction with NO. Nitrosyl hemeproteins also dissociate NO by photolysis.[22,23] However, the NO dissociation yields and the mechanism for the NO rebinding of hemeproteins are markedly different from those of the synthetic MP.[11,22−24] The proteins surrounding the heme control both the NO dissociation yields and the chemical reaction between NO and the central iron atom in the hemoproteins.

The nitrosyl adducts of the synthetic MP dissolved in micellar solutions are surrounded by surfactant molecules. Thus, like nitrosyl hemeproteins, the NO adducts of the synthetic MP in the micellar solutions are located in the hydrophobic phase. The present paper reports the laser-photolysis studies of the NO adducts of the synthetic MP with central metals Fe^{II}, Co^{II}, and Mn^{II} in micellar solutions.

Experimental Section

Chlorocobalt(III) octaethylporphyrin, $ClCo^{III}$OEP (OEP = octaethylporphyrin), and chloromanganese(III) tetraphenylporphyrin, $ClMn^{III}$TPP (TPP = tetraphenylporphyrin), were synthesized and purified according to the literature.[25,26] Reagent-grade chlorohemin ($ClFe^{III}$Hem), cetyltrimethylammonium bromide (CTAB), and sodium dodecyl sulfate (SDS) were used as supplied. The concentrations of surfactants used in the present study are 1.0×10^{-2} M for CTAB and 8×10^{-2} M for SDS aqueous solutions. The critical micelle concentrations (cmcs) of CTAB and SDS are respectively 9.2×10^{-4} and 8×10^{-3} M.[27] It is confirmed by spectroscopic measurements that the MP are insoluble in water without surfactants.

The MP were dissolved in 8×10^{-2} M SDS or 1.0×10^{-2} M CTAB aqueous solutions. For preparation of the NO adducts, the sample solutions were degassed, and then NO gas was introduced on a vacuum line. The NO concentrations in micellar solutions are determined from the NO partial pressure and the

* To whom correspondence should be addressed. Fax: 048-462-4668. Phone: 048-467-9426. E-mail: hoshino@postman.riken.go.jp.

10.1021/jp002515i CCC: $20.00
Published on Web 12/15/2000

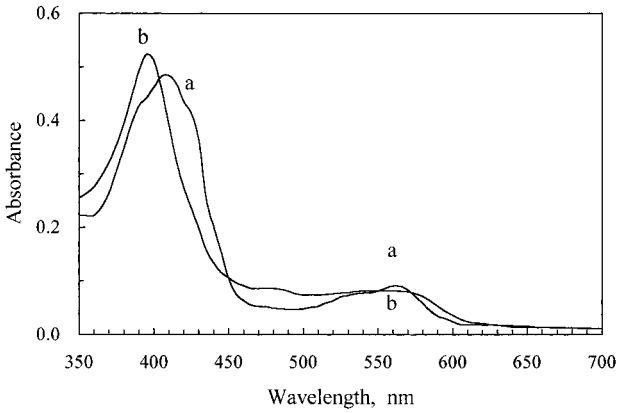

Figure 1. Absorption spectra of (a) Fe^{II}Hem and (b) (NO)Fe^{II}Hem in a 1.0×10^{-2} M CTAB micellar solution.

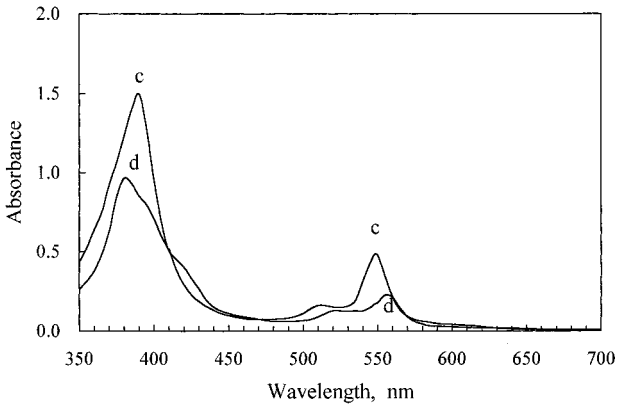

Figure 2. Absorption spectra of (c) Co^{II}OEP and (d) (NO)Co^{II}OEP in an 8.0×10^{-2} M SDS aqueous micellar solution.

Bunsen coefficient of NO in an aqueous solution (4.71×10^{-2} at 298 K).[28] Here we assume that the NO solubility in the aqueous phase of micellar solutions is the same as that in an aqueous solution.

Optical absorption and electron spin resonance (ESR) spectra were recorded on a Hitachi 330 spectrophotometer and Jeol FE-3A X-band spectrometer, respectively.

Laser-photolysis studies were carried out with the use of a Nd:YAG laser (HY 500 from JK Lasers, Ltd.) equipped with second (532 nm), third (355 nm), and fourth (266 nm) harmonic generators. The transient spectra were measured by the intensified charge-coupled device detector (DH 520-18F-01 from Andor Technology, Ltd.). For monitoring the decay of the transient absorption, the output from the photomultiplier (R758 from Hamamatsu Photonics) was conducted to the digital storage oscilloscope (Gould model 630 from Gould Instrument System, Ltd.).

Results

Optical Absorption and ESR Spectra. ClFe^{III}Hem was found to be soluble in a CTAB micellar solution. The spectrum exhibits an absorption band at 398 nm with a shoulder at 365 nm and a broad band centered at 580 nm. The molar absorption coefficient (ϵ) at 398 nm is determined to be 6.69×10^4 M^{-1} cm^{-1}.

ClFe^{III}Hem in the degassed CTAB micellar solution was reduced by sodium dithionite. Fe^{II}Hem, thus obtained, shows the absorption peak at 400 nm in the Soret band region. The micellar solution of Fe^{II}Hem was exposed to NO at 200 Torr to make the nitrosyl adducts.[5]

$$Fe^{II}Hem + NO \rightarrow (NO)Fe^{II}Hem \quad (1)$$

Figure 1 shows the absorption spectra of Fe^{II}Hem and (NO)-Fe^{II}Hem in CTAB micellar solutions. The spectrum of (NO)-Fe^{II}Hem has a sharp absorption peak at 396 nm ($\epsilon = 6.08 \times 10^4$ M^{-1} cm^{-1}). The ESR spectrum of (NO)Fe^{II}Hem in the micellar solution taken at 77 K was found to exhibit three well-resolved superhyperfine lines due to the nitrogen atom of the axial NO.[29,30]

When the degassed micellar solution of ClFe^{III}Hem was exposed to NO gas at 200 Torr, a new spectrum with a maximum peak at 396 nm appeared. The absorption spectrum was completely identical with that of (NO)Fe^{II}Hem produced by the nitrosylation of Fe^{II}Hem. The ESR spectra of the NO-exposed solutions of both ClFe^{III}Hem and Fe^{II}Hem at 77 K were the same. These results indicate that ClFe^{III}Hem in a CTAB micellar solution readily undergoes the reductive nitrosylation to produce (NO)Fe^{II}Hem.[31,32]

$$ClFe^{III}Hem + 2NO + H_2O \rightarrow (NO)Fe^{II}Hem + HONO + HCl \quad (2)$$

ClFe^{III}Hem was found to be insoluble in SDS micellar solutions. Neither ClFe^{III}TPP nor ClFe^{III}OEP was soluble in the CTAB or SDS micellar solutions.

An SDS micellar solution of ClCo^{III}OEP shows absorption peaks at 409 ($\epsilon = 1.09 \times 10^5$ M^{-1} cm^{-1}), 520, and 555 nm. When a small amount of sodium dithionite is added into the degassed SDS micellar solution, ClCo^{III}OEP is readily reduced to yield Co^{II}OEP. The spectrum of Co^{II}OEP in the solution has peaks at 390 ($\epsilon = 6.33 \times 10^4$ M^{-1} cm^{-1}), 510, and 548 nm. The micellar solution of Co^{II}OEP was exposed to NO gas at 200 Torr to produce (NO)Co^{II}OEP.

$$Co^{II}OEP + NO \rightarrow (NO)Co^{II}OEP \quad (3)$$

Figure 2 shows the absorption spectra of Co^{II}OEP and (NO)-Co^{II}OEP in SDS micellar solutions. The spectrum of (NO)Co^{II}-OEP exhibits absorption peaks at 380 nm ($\epsilon = 5.2 \times 10^4$ M^{-1} cm^{-1}) with a shoulder at 400 nm in the Soret band region and at 525 and 557 nm in the Q-band region.

The degassed micellar solution of ClCo^{III}OEP was exposed to NO gas at 200 Torr. The absorption spectrum measured after exposure to NO gas is found to be identical with that of (NO)-Co^{II}OEP. Thus, as in the case of ClFe^{III}Hem, ClCo^{III}OEP reacts with NO to give (NO)Co^{II}OEP by the reductive nitrosylation reaction.[12]

$$ClCo^{III}OEP + 2NO + H_2O \rightarrow (NO)Co^{II}OEP + HONO + HCl \quad (4)$$

ClCo^{III}OEP was found to be insoluble in cationic CTAB micellar solutions. ClCo^{III}TPP was insoluble in both anionic SDS and cationic CTAB micellar solutions.

ClMn^{III}TPP dissolved in an SDS micellar solution has absorption peaks at 385 ($\epsilon = 5.51 \times 10^4$ M^{-1} cm^{-1}), 479, 570, and 605 nm. Mn^{II}TPP obtained by reduction of ClMn^{III}TPP with sodium dithionite shows absorption peaks at 433 ($\epsilon = 4.12 \times 10^5$ M^{-1} cm^{-1}), 570, and 608 nm. When the solution of Mn^{II}-TPP is exposed to NO gas at 200 Torr, (NO)Mn^{II}TPP is produced.[33]

$$Mn^{II}TPP + NO \rightarrow (NO)Mn^{II}TPP \quad (5)$$

Figure 3 shows the absorption spectra of Mn^{II}TPP and (NO)-Mn^{II}TPP in SDS micellar solutions. The absorption spectrum

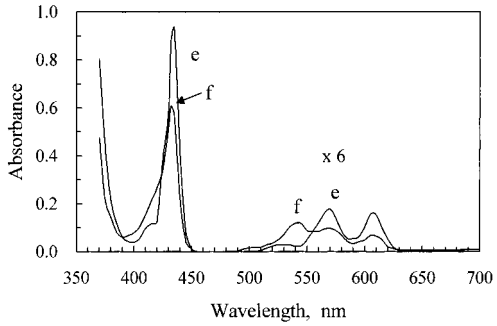

Figure 3. Absorption spectra of (e) $Mn^{II}TPP$ and (f) $(NO)Mn^{II}TPP$ in an 8.0×10^{-2} M SDS aqueous micellar solution.

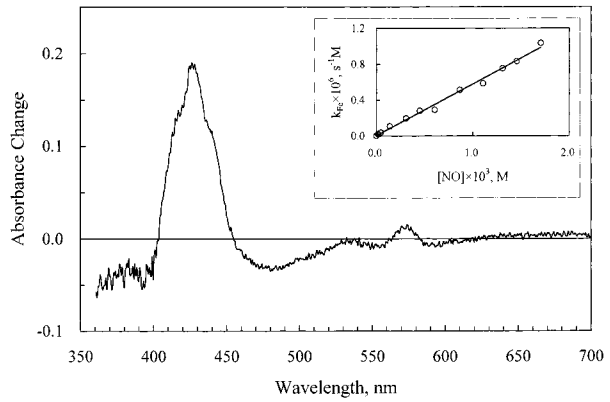

Figure 4. Transient absorption spectrum observed for $(NO)Fe^{II}Hem$ in a 1.0×10^{-2} M CTAB micellar solution at 20 ns after the 355 nm laser pulse. The inset shows the plot of the pseudo-first-order rate constant, k_{Fe}, represented as a function of $[NO_{aq}]$.

of $(NO)Mn^{II}TPP$ exhibits absorption peaks at 432 ($\epsilon = 2.00 \times 10^5$ M^{-1} cm^{-1}), 543, 575, and 608 nm.

$ClMn^{III}TPP$ in the CTAB micellar solution exhibits no absorption spectral changes by exposure to NO gas, suggesting that, unlike $ClFe^{III}Hem$ and $ClCo^{III}OEP$, $ClMn^{III}TPP$ does not react with NO.

Laser Photolysis of Nitrosyl Porphyrins in Micellar Solutions. Figure 4 shows the transient absorption spectrum observed for $(NO)Fe^{II}Hem$ in a 1.0×10^{-2} M CTAB micellar solution at 20 ns after the 355 nm laser pulse. The transient spectrum is in good agreement with the difference spectrum obtained by subtracting the spectrum of $(NO)Fe^{II}Hem$ from that of $Fe^{II}Hem$. This result indicates that NO is photodissociated from $(NO)Fe^{II}Hem$ by the 355 nm laser pulse.

$$(NO)Fe^{II}Hem + h\nu \rightarrow NO + Fe^{II}Hem \qquad (6)$$

The transient uniformly decays according to eq 1 in the whole wavelength region studied.

The decay of the transient $Fe^{II}Hem$ follows pseudo-first-order kinetics in the NO partial-pressure range of ca. 10−610 Torr. As shown in the inset of Figure 4, the plot of the pseudo-first-order rate constant k_{Fe} vs $[NO_{aq}]$ gives a straight line with an intercept at the origin.

$$k_{Fe} = k_{FeNO}(\text{pseudo})\,[NO_{aq}] \qquad (7)$$

The slope of the line gives the bimolecular rate constant k_{FeNO}(pseudo) for the reaction between $Fe^{II}Hem$ and NO: $k_{FeNO}(\text{pseudo}) = 5.7 \times 10^8$ M^{-1} s^{-1}.

Figure 5 shows the transient absorption spectrum observed at 20 ns for the 8.0×10^{-2} M SDS micellar solution of $(NO)Co^{II}OEP$ after the 355 nm laser pulse. The transient spectrum

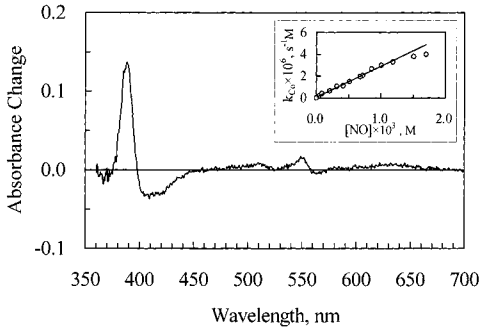

Figure 5. Transient absorption spectrum observed for $(NO)Co^{II}OEP$ in a 8.0×10^{-2} M SDS aqueous micellar solution at 20 ns after the 355 nm laser pulse. The inset exhibits the plot of the pseudo-first-order rate constant, k_{Co}, represented as a function of $[NO_{aq}]$.

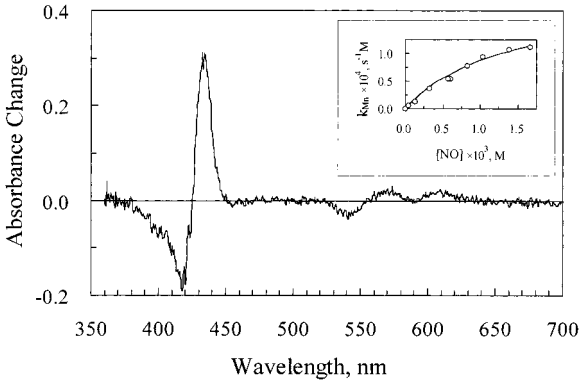

Figure 6. Transient absorption spectrum observed for $(NO)Mn^{II}TPP$ in a 8.0×10^{-2} M SDS aqueous micellar solution at 20 ns after the 355 nm laser pulse. The inset exhibits the plot of the pseudo-first-order rate constant, k_{Mn}, represented as a function of $[NO_{aq}]$.

is identical with the difference spectrum ($Co^{II}OEP$ minus $(NO)Co^{II}OEP$), indicating that NO is photodissociated from $(NO)Co^{II}OEP$.

$$(NO)Co^{II}OEP + h\nu \rightarrow NO + Co^{II}OEP \qquad (8)$$

$Co^{II}OEP$ thus produced reacts with NO according to eq 3, returning to $(NO)Co^{II}OEP$. The decay of the transient spectrum follows pseudo-first-order kinetics in the presence of excess NO. The inset of Figure 5 shows the plot of the pseudo-first-order rate constant k_{Co} represented as a function of [NO]. The slope of the line gives 2.82×10^9 M^{-1} s^{-1} as a bimolecular rate constant, k_{CoNO}(pseudo), for the reaction between $Co^{II}OEP$ and NO.

Figure 6 shows the transient spectrum observed at 20 ns for an 8×10^{-2} M SDS micellar solution of $(NO)Mn^{II}TPP$ after the 355 nm laser pulse. The transient spectrum is identical with the difference spectrum ($Mn^{II}TPP$ minus $(NO)Mn^{II}TPP$).

$$(NO)Mn^{II}TPP + h\nu \rightarrow NO + Mn^{II}TPP \qquad (9)$$

The transient $Mn^{II}TPP$ reacts with excess NO (eq 5) according to pseudo-first-order kinetics. The inset of Figure 6 shows the plot of the pseudo-first-order decay rate constant k_{Mn} represented as a function of [NO]. The rate constant k_{Mn} increases with an increase in [NO] and asymptotically approaches a limiting value. The apparent bimolecular rate constant k_{MnNO}(pseudo) for the reaction of $Mn^{II}TPP$ with NO is obtained as 1.56×10^7 M^{-1} s^{-1} from the initial slope of the plot of k_{Mn} vs [NO] obtained at $[NO] < 6.0 \times 10^{-4}$ M.

Bimolecular Rate Constants in the Absence of Excess NO. As mentioned above, the second-order rate constants k_{MNO}-

TABLE 1: Bimolecular Rate Constants k_{MNO}(pseudo) and k_{MNO}(second) for the Nitrosylation Reaction of MP

	$Co^{II}OEP$,[a] $M^{-1}\ s^{-1}$	$Fe^{II}Hem$,[b] $M^{-1}\ s^{-1}$	$Mn^{II}TPP$,[a] $M^{-1}\ s^{-1}$
k_{MNO}(pseudo)	2.82×10^9	5.7×10^8	1.56×10^7
k_{MNO}(second)	1.52×10^9	2.26×10^8	5.0×10^7[c]

[a] 8×10^{-2} M SDS micellar solution. [b] 1.0×10^{-2} M CATB micellar solution. [c] This value is roughly estimated from the slope of the plot k_{MnNO}(pseudo) vs [NO] in the range of $0 < [NO] < 3.0 \times 10^{-4}$ M.

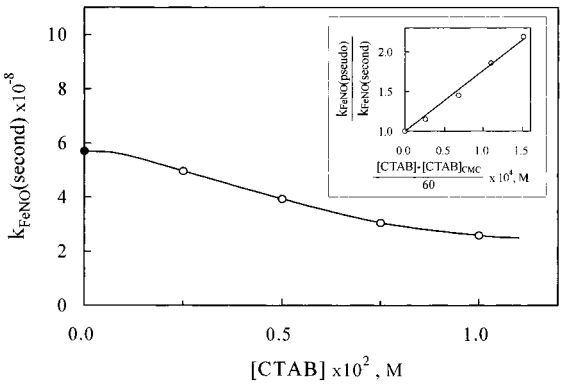

Figure 7. Second-order rate constant, k_{CoNO}(second), represented as a function of [CTAB]. The inset shows the plot of k_{CoNO}(pseudo)/k_{CoNO}(second) vs [micelle]$_{CTAB}$ (see text).

(pseudo) (M = Fe, Co, and Mn) for the reaction between NO and metalloporphyrin can be determined from the pseudo-first-order rate constants, k_M (M = Fe, Co, and Mn), obtained in the presence of excess NO: the slope of the plot of k_M vs [NO] gives k_{MNO}(pseudo). The second-order rate constants can also be determined with laser photolysis of nitrosyl porphyrins in the absence of excess NO. The decay of the MP produced by laser photolysis was found to follow second-order kinetics with the rate constants k_{MNO}(second) (M = Fe^{II}, Co^{II}, and Mn^{II}).

$$(\Delta D_\lambda)^{-1} = (\Delta D_\lambda^0)^{-1}[-k_{MNO}(\text{second})/\Delta\epsilon_\lambda]t \qquad (10)$$

Here, ΔD_λ^0 and ΔD_λ (λ = monitoring wavelength) are respectively the absorbance changes of the transient spectrum at times zero and t after the laser pulse. $\Delta\epsilon_\lambda$ is the difference in the molar absorption coefficient of the metalloporphyrin and the nitrosyl metalloporphyrin.

In Table 1 are listed the bimolecular rate constants k_{MNO}(pseudo) and k_{MNO}(second) (M = Fe^{II}, Co^{II}, and Mn^{II}) obtained for the reaction between MP and NO in 1.0×10^{-2} M CTAB and 8.0×10^{-2} M SDS micellar solutions. It is noteworthy that the values of k_{MNO}(pseudo) are significantly different from those of k_{MNO}(second).

For $Co^{II}OEP$ and $Fe^{II}Hem$, k_{MNO}(pseudo) is much larger than k_{MNO}(second). However, $Mn^{II}TPP$ gives k_{MnNO}(pseudo) < k_{MnNO}(second). These results are discussed later on the basis of the reaction mechanism for the nitrosylation of MP in micellar solutions: the nitrosylation mechanism of $Mn^{II}TPP$ is very different from those of $Fe^{II}TPP$ and $Co^{II}TPP$.

The rate constants k_{FeNO}(second) and k_{CoNO}(second) were measured by changing the concentrations of CTAB and SDS in aqueous solutions. Figure 7 shows the plot of k_{FeNO}(second) represented as a function of [CTAB]. With a decrease in [CTAB], k_{FeNO}(second) becomes larger and approaches the limiting value, k_{FeNO}(pseudo). As will be shown later, this result suggests that the "effective" [NO] concentration responsible for the nitrosylation decreases with an increase in the micelle concentrations.

TABLE 2: Quantum Yields for the Photodissociation of NO from Nitrosyl Porphyrins in Micellar and Toluene Solutions Determined by 355 nm Laser Photolysis

	(NO)$Co^{II}OEP$	(NO)$Fe^{II}Hem$	(NO)$Mn^{II}TPP$
micelle	0.55 (±0.05)	0.15 (±0.01)	0.21 (±0.02)
toluene	1.0 (±0.05)[a]	0.5 (±0.05)[a,b]	0.78 (±0.05)[a]

[a] Reference 5. [b] (NO)$Fe^{II}Hem$ is insoluble in toluene. For a comparison with others, the quantum yield for photoinduced denitrosylation of (NO)$Fe^{II}TPP$ in toluene[5] is given in the table.

Similarly, the plot of k_{CoNO}(second) vs [SDS] demonstrates that k_{CoNO}(second) increases with a decrease in [SDS] and approaches k_{CoNO}(pseudo) on going to low concentration of SDS.

Quantum Yield Measurements. The quantum yields for the photodissociation of NO from nitrosyl MP, (NO)MP, in micellar solutions were determined with the use of the 355 nm laser-photolysis method. The details are described previously.[2] Actinometry was carried out with the use of a benzene solution of benzophenone. The laser photolysis of benzophenone at 355 nm gives the triplet benzophenone with the quantum yield of unity, $\phi_T = 1.0$.[34] The molar absorption coefficient of the triplet benzophenone in benzene has been determined as $\epsilon_T = 7.6 \times 10^3\ M^{-1}\ cm^{-1}$ at 530 nm.[34] The micellar solution of (NO)MP is adjusted to have an absorbance identical with that of the benzophenone solution at 355 nm. When the micellar solution is subjected to a 355 nm laser pulse, the absorbance change $\Delta D_{MP}(\lambda)$ monitored at λ for the formation of MP is detected at 20 ns after the pulse. Similarly, the benzene solution of benzophenone gives the triplet benzophenone with the absorbance at 530 nm, ΔD_{BP}(530 nm), after the pulse. Then, the quantum yield, ϕ_{NO}, for photoinduced denitrosylation of (NO)MP is represented as

$$\phi_{NO} = \epsilon_T \Delta D_{MP}(\lambda)/\Delta\epsilon_T(\lambda)\ \Delta D_{BP}(530\ \text{nm}) \qquad (11)$$

Here $\Delta\epsilon_T(\lambda)$ is the difference in the molar absorption coefficient between MP and (NO)MP at the wavelength λ in the micellar solution. The quantum yields, ϕ_{NO}, thus obtained are 0.15 (±0.01) for (NO)$Fe^{II}Hem$, 0.55 (±0.05) for (NO)$Co^{II}OEP$, and 0.21(±0.02) for (NO)$Mn^{II}TPP$. It is found that the quantum yields are independent of the NO pressures in the range 0−600 Torr.

In Table 2 are listed the quantum yields for the photodissociation of NO from nitrosyl porphyrins in both micellar solutions and toluene. The dissociation yields in toluene solutions are 2−4 times larger than those in micellar solutions.

Discussion

Methemoglobin, metmyoglobin, and ferric cytochrome *c* undergo reductive nitrosylation to yield their NO adducts of the reduced forms.[31] Such reductive nitrosylation takes place when the synthetic Fe^{III} and Co^{III} porphyrins in alcohol are exposed to NO gas.[2,32] The present study shows that Fe^{III} and Co^{III} porphyrins undergo reductive nitrosylation even in micellar solutions to give the nitrosyl adducts of Fe^{II} and Co^{II} porphyrins.

The present laser-photolysis studies demonstrate that (NO)MP photodissociate NO in micellar solutions. The quantum yields for full photodissociation of NO in micellar solutions are larger than those of nitrosyl hemoproteins.[11] Probably, unlike the proteins of hemoglobin and myoglobin, micelles have no trapping site of NO: the photodissociated NO freely diffuses into the aqueous phase.

The kinetic studies on the nitrosylation of MP in solutions have been extensively studied by means of a laser-flash-photolysis technique. In Table 3 are listed the bimolecular rate

TABLE 3: Bimolecular Rate Constants k_{MNO}(pseudo) for the Nitrosylation Reaction of MP in Benzene, Ethanol, and Micellar Solutions

	benzene, M^{-1} s^{-1}	ethanol, M^{-1} s^{-1}	micelle k_{MNO}(pseudo), M^{-1} s^{-1}
$Co^{II}OEP$	2.3×10^{9} [a]	2.98×10^{9}	2.82×10^{9}
$Fe^{II}Hem$	insoluble	1.42×10^{9}	5.7×10^{8}
$Mn^{II}TPP$	5.3×10^{8} [a]	4.90×10^{5} [b]	1.56×10^{7}

[a] Reference 5. [b] Reference 2.

constants for the nitrosylation of MP in benzene, ethanol, and micellar solutions.

The bimolecular rate constant for the nitrosylation of $Co^{II}OEP$ in the SDS micellar solution is almost identical with those in toluene and ethanol. In the case of $Mn^{II}TPP$, the smallest rate constant is given in ethanol. This has been interpreted in terms of the strong coordination of solvent ethanol molecules to the axial positions of $Mn^{II}TPP$.[2]

An interesting finding in the present study is that the values of k_{MNO}(pseudo) are significantly different from those of k_{MNO}(second). The (NO)MP dissolved in micelles dissociate NO by laser flash photolysis, leaving the MP in micelles. The plots of both k_{Fe} vs [NO] and k_{Co} vs [NO] give straight lines. However, the plot of k_{Mn} vs [NO] tends to level off at a higher concentration of NO. This result indicates that the nitrosylation mechanism of $Mn^{II}TPP$ is very different from those of Co^{II}-OEP and $Fe^{II}Hem$. We, thus, initially discuss the nitrosylation mechanism of $Co^{II}OEP$ and $Fe^{II}Hem$.

NO molecules are soluble in both aqueous and hydrocarbon solutions. In micellar solutions, NO molecules in the aqueous phase, NO_{aq}, are in equilibrium with those trapped in micelles, $NO_{micelle}$.

$$NO_{aq} + \text{micelle} \overset{K}{\rightleftharpoons} NO_{micelle} \tag{12}$$

$$K = ([NO_{micelle}]/[NO_{aq}])[\text{micelle}] \tag{13}$$

The MP, $M^{II}P_{micelle}$, in micellar solutions produced by photolysis of $(NO)M^{II}P_{micelle}$ react with both NO_{aq} and $NO_{micelle}$. Thus, the nitrosylation reaction of $M^{II}P_{micelle}$ is represented by

$$M^{II}P_{micelle} + NO_{aq} \xrightarrow{k_{aq,M}} (NO)M^{II}P_{micelle} \tag{14}$$

$$M^{II}P_{micelle} + NO_{micelle} \xrightarrow{k_{micelle,M}} (NO)M^{II}P_{micelle} \tag{15}$$

The concentration of NO produced by photolysis of (NO)-$M^{II}P_{micelle}$ in the absence of excess NO is very low ($<10^{-5}$ M) in comparison with the concentration of micelles. Presumably, one micelle traps one NO molecule photodissociated. From eqs 13−15, the bimolecular rate constants k_{MNO}(second) obtained by the second-order decay of the transient porphyrins are expressed as

$$k_{MNO}(\text{second}) = k_{aq,M}/(1 + K[\text{micelle}]) + k_{micelle,M}K[\text{micelle}]/(1 + K[\text{micelle}]) \tag{16}$$

Equation 16 implies that the rate constant k_{MNO}(second) is composed of two terms: the first term in eq 16 is the rate constant for the reaction between $MP^{II}_{micelle}$ and NO in the aqueous phase, and the second term, the rate constant between $MP^{II}_{micelle}$ and $NO_{micelle}$. Here we assume that $k_{micelle,M}$ is very small in comparison with $k_{aq,M}$ because of the electrostatic repulsion between micelles. Equation 16, thus, is represented as

$$k_{MNO}(\text{second}) = k_{aq,M}/(1 + K[\text{micelle}]) \tag{17}$$

In the presence of excess NO, the pseudo-first-order rate constant k_M is derived from eqs 14 and 15.

$$k_M = k_{aq,M}[NO_{aq}] + k_{micelle,M}[NO_{micelle}] \tag{18}$$

Here again, we assume that $k_{micelle,M}$ is negligibly small, owing to the electrostatic repulsion between micelles. Thus, eq 18 is readily transformed to

$$k_M = k_{aq,M}[NO_{aq}] \tag{19}$$

where $[NO_{aq}]$ is calculated from the Bunsen coefficient of NO and the partial pressure of NO. In fact, as shown in the insets of Figures 4 and 5, the plot of k_M vs $[NO_{aq}]$ gives a straight line for $Fe^{II}Hem$ and $Co^{II}OEP$. From the above consideration, the bimolecular rate constant k_{MNO}(pseudo) obtained in the presence of excess NO is expressed as

$$k_{MNO}(\text{pseudo}) = k_{aq,M} \tag{20}$$

Equations 17 and 20 lead to the following equation:

$$k_{MNO}(\text{second}) = k_{MNO}(\text{pseudo})/(1 + K[\text{micelle}]) \tag{21}$$

Because $K > 0$, eq 21 clearly indicates that k_{MNO}(pseudo) > k_{MNO}(second), which is in agreement with the present experimental data for $(NO)Fe^{II}Hem$ and $(NO)Co^{II}OEP$.

Equation 21 also explains well the plot of k_{FeNO}(second) vs [CTAB] shown in Figure 7. The molar concentration of the micelle, $[\text{micelle}]_{CTAB}$, of CTAB is assumed to be expressed as[28]

$$[\text{micelle}]_{CTAB} = ([CTAB] - [CTAB]_{cmc})/N \tag{22}$$

where $[CTAB]_{cmc}$ and N are the cmc concentration and the number of aggregations of CTAB, respectively. Because $N = 60$ and $[CTAB]_{cmc} = 9.2 \times 10^{-4}$ M for CTAB,[28] we obtain

$$k_{FeNO}(\text{pseudo})/k_{FeNO}(\text{second}) = 1 + K([CTAB] - [CTAB]_{cmc})/60 \tag{23}$$

As shown in the inset of Figure 7, the plot of k_{FeNO}(pseudo)/k_{FeNO}(second) vs $[\text{micelle}]_{CTAB}$ gives a straight line. From the slope of the line, K is determined to be 7.6×10^{3} M^{-1} for CTAB. Similarly, the K values of SDS are obtained as 9.2×10^{2} M^{-1} from the laser photolysis of $(NO)Co^{II}OEP$ in an aqueous SDS solution: the plot of k_{CoNO}(pseudo)/k_{CoNO}(second) vs $[\text{micelle}]_{SDS}$ gives a straight line ($N = 62$ for SDS). This value is 1 order of magnitude smaller than that obtained from CTAB.

The nitrosylation mechanism of $Mn^{II}TPP$ differs markedly from those of $Co^{II}OEP$ and $Fe^{II}Hem$. For interpretation of the leveling-off of k_{Mn} at high concentrations of $[NO_{aq}]$, we assume the following reaction mechanism in micellar solutions:

$$Mn^{II}TPP(H_2O)_{2,micelle} \underset{k_a[H_2O]}{\overset{k_d}{\rightleftharpoons}} Mn^{II}TPP(H_2O)_{micelle} + H_2O \tag{24}$$

$$Mn^{II}TPP(H_2O)_{micelle} + NO_{aq} \overset{k_{aq,Mn}}{\rightleftharpoons} (NO)Mn^{II}TPP(H_2O)_{micelle} \tag{25}$$

$$Mn^{II}TPP(H_2O)_{micelle} + NO_{micelle} \overset{k_{micelle,Mn}}{\rightleftharpoons} (NO)Mn^{II}TPP(H_2O)_{micelle} \quad (26)$$

$Mn^{II}TPP$ yielded by photolysis of (NO)MnTPP readily reacts with water to give $Mn^{II}TPP(H_2O)_2$, which is in equilibrium with $Mn^{II}TPP(H_2O)$ (eq 24). NO_{aq} is assumed to react solely with $Mn^{II}TPP(H_2O)$, because if the two axial positions are occupied by water molecules, $Mn^{II}TPP(H_2O)_2$ is unable to react with NO. This is further supported by an earlier observation that the rate constant for the nitrosylation of $Mn^{II}TPP$ in ethanol is 3 orders of magnitude smaller than that in noncoordinating solvent toluene.[2]

The rate constants k_{MnNO}(second) and k_{Mn} are obtained from the combination of eqs 13 and 24−26. In the absence of excess NO, the equilibrium reaction shown in eq 23 is assumed to hold during the course of the nitrosylation reaction because of the low concentration of NO photodissociated. Then, the rate constant k_{MnNO}(second) is expressed as

$$k_{MnNO}(\text{second}) = \frac{k_{aq,Mn} + k_{micelle,Mn}K[\text{micelle}]_{SDS}}{1 + K[\text{micelle}]_{SDS}} \frac{k_a[H_2O] + k_d}{k_a[H_2O]} \quad (27)$$

In the presence of excess NO, the equilibrium in eq 23 does not hold during the nitrosylation. By using a steady-state approximation with regard to $Mn^{II}TPP(H_2O)$, the pseudo-first-order rate constant, k_{Mn}, is expressed as

$$k_{Mn} = \frac{k_d(k_{aq,Mn} + k_{micelle,Mn}K[\text{micelle}]_{SDS})[NO_{aq}]}{k_a[H_2O] + (k_{aq,Mn} + k_{micelle,Mn}K[\text{micelle}]_{SDS})[NO_{aq}]} \quad (28)$$

Equation 28 explains well the plot of k_{Mn} vs $[NO_{aq}]$ shown in Figure 6: the leveling-off of k_{Mn} at a higher concentration of NO is interpreted by assuming that the rate-determining step for the nitrosylation of $Mn^{II}TPP(H_2O)_2$ is the dissociation of the axial H_2O.

Transformation of eq 28 gives

$$k_{Mn}^{-1} = \{k_a[H_2O]/k_d(k_{aq,Mn} + k_{micelle,Mn}K[\text{micelle}]_{SDS})\}[NO_{aq}]^{-1} + k_d^{-1} \quad (29)$$

The plot of k_{Mn}^{-1} vs $[NO_{aq}]^{-1}$ gives a straight line. The slope and the intercept of the line respectively give

$$k_a[H_2O]/k_d(k_{aq,Mn} + k_{micelle,Mn}K[\text{micelle}]_{SDS}) = 6.4 \times 10^{-8}\ \text{M s} \quad (30)$$

and $k_d = 2.06 \times 10^4\ s^{-1}$. Equations 27 and 30 lead to

$$6.4 \times 10^{-8} \times k_{Mn}(\text{second}) = (k_a[H_2O] + k_d)/k_d(1 + K[\text{micelle}]_{SDS}) \quad (31)$$

With the use of k_{Mn}(second) $= 5.7 \times 10^7\ s^{-1}$, $k_d = 2.06 \times 10^4\ s^{-1}$, $[\text{micelle}]_{SDS} = 1.16 \times 10^{-3}$ M, and $K = 9.2 \times 10^2\ M^{-1}$ obtained from $Co^{II}OEP$ in SDS micellar solutions, $k_a[H_2O]$ is calculated as $1.4 \times 10^5\ s^{-1}$. Equation 28 gives the apparent pseudo-first-order rate constant k_{Mn}(pseudo).

$$k_{Mn}(\text{pseudo}) = k_d(k_{aq,Mn} + k_{micelle,Mn}K[\text{micelle}]_{SDS})/k_a[H_2O] \quad (32)$$

From eqs 27 and 32, we obtain

$$k_{Mn}(\text{pseudo})/k_{Mn}(\text{second}) = k_d(1 + K[\text{micelle}]_{SDS})/(k_a[H_2O] + k_d) \quad (33)$$

By using k_d, K, and $k_a[H_2O]$ obtained above, k_{Mn}(pseudo)/k_{Mn}(second) is determined as 0.27. This value is in moderate agreement with that (0.31) calculated from Table 1. From these considerations, it is concluded that the leveling-off observed for k_{Mn} at higher concentrations of NO is not ascribed to the effects of the micelle on the nitrosylation reaction of $Mn^{II}TPP$. The leveling-off originates from the reaction mechanism for the nitrosylation of $Mn^{II}TPP$: the rate-determining step for the nitrosylation reaction is the dissociation of an axial water from $Mn^{II}TPP(H_2O)_2$.

Summary

The laser-photolysis studies of nitrosyl porphyrins revealed that the quantum yields for the photodissociation of NO in micellar solutions are smaller than those in toluene solutions, suggesting that the geminate recombination between NO and MP in the micelles occur more efficiently than in toluene.

The reaction mechanism for the nitrosylation of $Mn^{II}TPP$ is different from that of $Co^{II}OEP$ and $Fe^{II}Hem$. For the former, the major species in micellar solution is the six-coordinate species, $Mn^{II}TPP(H_2O)_{2,micelle}$, which is unable to react with NO. The kinetic study reveals that the rate-determining step for the nitrosylation is the dissociation of the axial water from $Mn^{II}TPP(H_2O)_{2,micelle}$. The five-coordinate species, $Mn^{II}TPP(H_2O)$, thus produced reacts with NO to yield (NO)MnTPP. On the other hand, the major species of $Co^{II}OEP$ and $Fe^{II}Hem$ in micellar solutions are considered to be the four- or five-coordinate species which readily react with NO.

The bimolecular rate constants k_M(pseudo) (M = Co and Fe) obtained from the plot of k_M vs [NO] markedly differ from k_M(second) determined from the second-order decay of $MP_{micelle}$ in the absence of excess NO. This result is well-explained by assuming that (1) NO molecules trapped in micelles are in equilibrium with those in the aqueous phase, (2) MP reacts with NO in the aqueous phase, and (3) NO molecules in micelles are unable to react with $MP_{micelle}$ because of the electrostatic repulsion between micelles.

References and Notes

(1) James, B. R. In *The Porphyrins*; Dolphin, D., Ed.; Academic Press: New York, 1978; Vol. V, Chapter 6.
(2) Hoshino, M.; Nagashima, Y.; Seki, H.; De Leo, M.; Ford, P. C. *Inorg. Chem.* **1998**, *37*, 2464−2469.
(3) Hoffman, B. M.; Weschler, C. J.; Basolo, F. *J. Am. Chem. Soc.* **1976**, *98*, 5473−5482.
(4) Collman, J. P.; Gagne, R. R.; Reed, C. A.; Halbert, J. R.; Lang, G.; Robinson, W. T. *J. Am. Chem. Soc.* **1975**, *97*, 1427−1439.
(5) Hoshino, M.; Kogure, M. *J. Phys. Chem.* **1989**, *93*, 5478−5484.
(6) White, D. K.; Cannon, J. B.; Traylor, T. G. *J. Am. Chem. Soc.* **1979**, *101*, 2443−2454.
(7) Hoffman, B. M.; Gibson, Q. H. *Proc. Natl. Acad. Sci. U.S.A.* **1978**, *75*, 21−25.
(8) Hoshino, M.; Ueda, K.; Takahashi, M.; Yamaji, M.; Hama, Y.; Miyazaki, Y. *J. Phys. Chem.* **1992**, *96*, 8894−8869.
(9) Hoshino, M.; Baba, T. *J. Am. Chem. Soc.* **1998**, *120*, 6820−6821.
(10) Parkhurst, L. J.; Gross, D. J. *Biochemistry* **1984**, *23*, 2180−2186.
(11) Hoshino, M.; Ozawa, K.; Seki, H.; Ford, P. C. *J. Am. Chem. Soc.* **1993**, *115*, 9568−9575.
(12) Hoshino, M.; Laverman, L.; Ford, P. C. *Coord. Chem. Rev.* **1999**, *187*, 75−102.
(13) Ignarro, L. J. A. *Rev. Pharmacol. Toxicol.* **1990**, *30*, 535−560.
(14) Cullota, E.; Koshland, D. E. *Science* **1992**, *258*, 1862−1865.
(15) Klatt, P.; Schmidt, K.; Uray, G.; Mayer, B. *J. Biol. Chem.* **1993**, *268*, 14781−14787.
(16) Shibuki, K.; Okada, D. *Nature* **1991**, *349*, 326−328.
(17) Hibbs, J. B., Jr.; Vavrin, Z.; Taintor, J. *J. Immunol.* **1987**, *138*, 550−565.

(18) Heck, D. E.; Laskin, D. L.; Gardner, C. R. *J. Biol. Chem*. **1992**, *267*, 21277−21280.
(19) Odaka, M.; Fujii, K.; Hoshino, M.; Noguchi, T.; Tsujimura, M.; Nagashima, S.; Yohda, M.; Nagamune, T.; Inoue, Y.; Endo, I. *J. Am. Chem. Soc*. **1997**, *119*, 3785−3791.
(20) Cleeter, M. W. J.; Cooper, J. M.; Darley-Usmar, V. M.; Moncada, S.; Scapira, A. H. V. *FEBS Lett*. **1994**, *395*, 50−54.
(21) Brown, G. C. *Eur. J. Biochem*. **1995**, *232*, 188−191.
(22) Petrich, J. W.; Lambry, J.-C.; Kuczera, K.; Karplus, M.; Poyart, C.; Martin, J. L. *Biochemistry* **1991**, *30*, 3975−3987.
(23) Cornelius, P. A.; Hochstrasser, R. M.; Steel, A. W. *J. Mol. Biol*. **1983**, *163*, 119−128.
(24) Morlino, E. A.; Rodgers, M. A. J. *J. Am. Chem. Soc*. **1996**, *118*, 11798−11804.
(25) Sakurai, T.; Yamamoto, K.; Naito, H.; Nakamoto, N. *Bull. Chem. Soc. Jpn*. **1975**, *97*, 6461−6466.
(26) Boucher, L. *J. Am. Chem. Soc*. **1968**, *90*, 6640−6645.
(27) Kalyanasundaram, K. *Photochemistry in Microheterogeneous Systems*; Academic Press: New York, 1987.
(28) Chihara, H. In *Kagakubinran*; Japan Chemical Society, Ed.; Maruzen: Tokyo, 1984; Vol. II, p 158.
(29) Yonetani, T.; Yamamoto, H.; Erman, J. E.; Leigh, J. S., Jr.; Reed, G. H. *J. Biol. Chem*. **1972**, *247*, 2447−2455.
(30) Kon, H.; Kataoka, N. *Biochemistry* **1969**, *8*, 4757−4762.
(31) Hoshino, M.; Maeda, M.; Konishi, R.; Seki, H.; Ford, P. C. *J. Am. Chem. Soc*. **1996**, *118*, 5702−5707.
(32) Wayland, B. B.; Olson, L. W. *J. Chem. Soc., Chem. Commun*. **1973**, 897−898.
(33) Hoshino, M.; Konishi, S. *Chem. Phys. Lett*. **1985**, *115*, 511−514.
(34) Bensasson, R.; Land, E. J. *Trans. Faraday Soc*. **1971**, *67*, 1904−1915.